
Article:
Zhu, Z-Q. orcid.org/0000-0001-7175-3307, Xue, S. orcid.org/0000-0003-4534-3878, Chu, W. et al. (4 more authors) (2019) Evaluation of Iron Loss Models in Electrical Machines. IEEE Transactions on Industry Applications, 55 (2). pp. 1461-1472. ISSN 0093-9994

https://doi.org/10.1109/TIA.2018.2880674

Evaluation of Iron Loss Models in Electrical Machines

Z. Q. Zhu, Shaoshen Xue and W. Q. Chu
University of Sheffield
Mappin Street
Sheffield S1 3JD, UK
xueshaoshen@hotmail.com

Jianghua Feng, Shuying Guo, Zhichu Chen and Jun Peng
CRRC Zhuzhou Institute Co. Ltd
Shidai Road, Shifeng District,
Zhuzhou, Hunan, 412001, China
fengjh@csrzic.com

***Abstract* -- In this paper, more than ten different iron loss models are experimentally evaluated, which cover alternating and rotating fields, influence of temperature, DC bias flux density and distorted flux density due to PWM inverter. Iron loss models considering alternating fields are evaluated by the measured results of a lamination ring specimen. The iron loss model considering rotating field and non-sinusoidal field are evaluated by the measured results of an electrical machine under different conditions. The iron loss models considering temperature influence are also evaluated by thermal analyses and experimental tests. Based on these comprehensive investigations, the iron loss models having the best prediction accuracy for each case are identified.**

***Index terms* -- Electrical machine, Iron loss, Thermal analysis.**

I. Introduction

Iron loss is one of the major losses in electrical machines. The accurate prediction of the iron loss is essential for the electromagnetic and thermal design of electrical machines. Many different iron loss models have been developed in [1]-[4]. These iron loss models are widely used since they have solid physical basis while very easy to implement [5]-[7]. Based on these iron loss models, many improvements have been done to adapt different conditions. In [8]-[10], the temperature dependency of the iron loss is investigated and then considered in the modified models. In [11]-[13], the additional iron loss introduced by DC bias flux density is modeled. The iron loss models developed in [14]-[16] consider the influence of flux density distortion, usually caused by pulse width modulation (PWM) inverters, on the iron loss. All the iron loss models in [1]-[16] are based on alternating flux density. However, in electrical machines, the flux density can be rotational. Different models have been developed in [17]-[18] to consider the influence of rotational field. Different iron loss models are evaluated and compared in [19]. However, no thermal evaluation is carried out, which is critical for electrical machine loss prediction. Furthermore, *B-H* loops under different temperatures should be measured to demonstrate the iron loss behaviour. Therefore, further loss and thermal evaluations based on both lamination and electrical machine tests are necessary to validate the effectiveness of the iron loss models in electrical machine design.

In this paper, more than ten different iron loss models are evaluated against the measured results. This paper is organized as follows. In Section II, the iron loss test method in steel lamination ring specimen is illustrated. Based on the ring specimen tests, different iron loss models for constant temperature are evaluated in Section III. In Section IV, the iron loss models considering temperature influence are evaluated by the ring specimen tests, the electrical machine loss and thermal tests. By selecting the most accurate iron loss model considering alternating flux density, the rotational field influence on the iron loss is discussed in Section V. Different iron loss models for rotational flux density are evaluated against the testing results of an electrical machine. In Section VI, different iron loss models considering nonsinusoidal flux density, i.e. DC bias flux density, and distortion caused by PWM inverter are also evaluated against the measurements on an electrical machine.

II. Iron Loss Test in Steel Lamination Specimen

The ring specimen iron loss test has been widely used to measure the iron loss of steel laminations under alternating flux density [20]-[24]. The measurement system is shown in Fig. 1. Table I shows the parameters of the ring specimen. The ring specimen is wounded by the excitation coil and the measuring coil. The excitation coil is supplied by an AC power source which is the California Instrument 4500iL in this paper. The measuring coil having the same number of turns with excitation coil is closely wounded together with the excitation coil and connected to the oscilloscope to measure the induced voltage. Thus, the voltage drop on the excitation coil's resistance is excluded in the measured induced voltage. The current in the excitation coil is measured by the Tektronix A622 current probe. The iron loss density p_{Fe}, the field strength $H(t)$ and the flux density $B(t)$ can be calculated as:

$$p_{\mathrm{Fe}} = \frac{1}{T\rho V}\int_0^T u(t)i(t)dt \tag{1}$$

$$H(t) = \frac{Ni(t)}{l_{\mathrm{eff}}} \tag{2}$$

$$B(t) = \frac{\int u(t)dt}{NA} \tag{3}$$

where p_{Fe} is the iron loss density. $u(t)$ is the instant induced voltage of the measuring coil. $i(t)$ is the instant current in the excitation coil. T is the time period of the current and the voltage. ρ and V are the mass density and the volume of the ring specimen, respectively. N is the number of turns of the excitation coil and the measuring coil. l_{eff} is the effective length of the ring specimen. A is the cross sectional area of the ring specimen.

In order to investigate the influence of temperature on the iron loss, the ring specimen can be heated by its own iron loss to the designate temperature. A K-type thermal couple is also installed to measure the temperature. Thus, iron loss under different temperatures can be obtained. The test range of the measuring system is also summarized in Table I.

Fig. 2 shows the measured iron loss in the ring specimen at different frequencies, flux densities and temperatures. The iron

losses vary in an identical pattern when the lamination temperature is 40°C and 100°C. This iron loss variation with flux density and frequency has been investigated and modelled widely in [1]-[4]. These iron loss models will be discussed and evaluated in Section III. On the other hand, the iron losses at 40°C and 100°C are different when the flux density and frequency are the same. In other word, the temperature influences the iron loss significantly. This phenomenon is investigated in [8] and modelled in [9] and [10]. Fig. 3 shows the measured *B-H* loops at different temperatures and frequencies. Fig. 4 shows the *B-H* loops at different temperatures and frequencies on the flux density saturation level. It can be seen that the shapes of *B-H* loops vary with frequency and temperature. The iron losses are then affected. The iron loss models for considering the temperature influence will be discussed in Section IV.

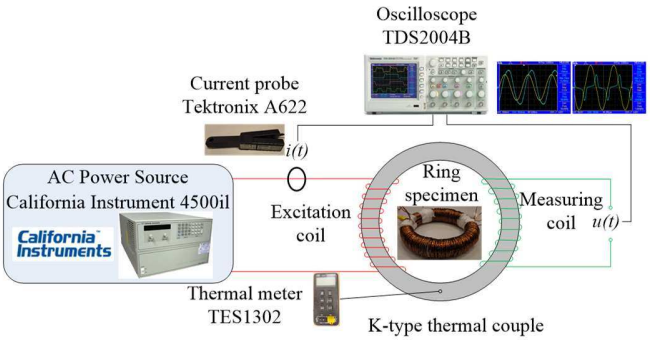

Fig. 1. Schematic diagram of ring specimen iron loss measurement.

TABLE I
PARAMETERS OF RING SPECIMEN

Type of silicon steel lamination		V300-35A
Thickness of single lamination	mm	0.35
Outer diameter of ring specimen	mm	150
Inner diameter of ring specimen	mm	125
Effective thickness of ring specimen	mm	14
No. of turns for excitation and measuring coils *N*		102
Maximum output voltage in RMS value	V	150
Maximum output current in RMS value	A	30
Frequency range	Hz	50-1000
Temperature range	°C	40-100

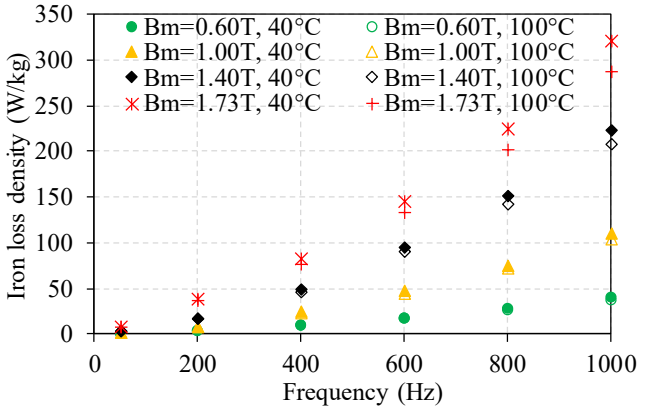

Fig. 2 Measured iron loss in the ring specimen at different frequency, flux density and temperature.

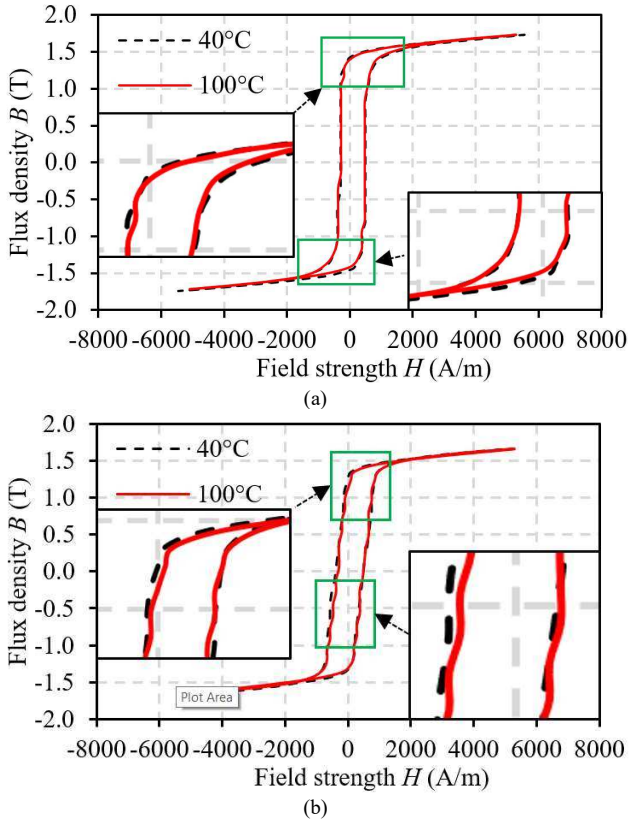

Fig. 3. *B-H* loops at different frequencies and temperatures when flux density is sinusoidal. (a) 50Hz. (b) 1000Hz.

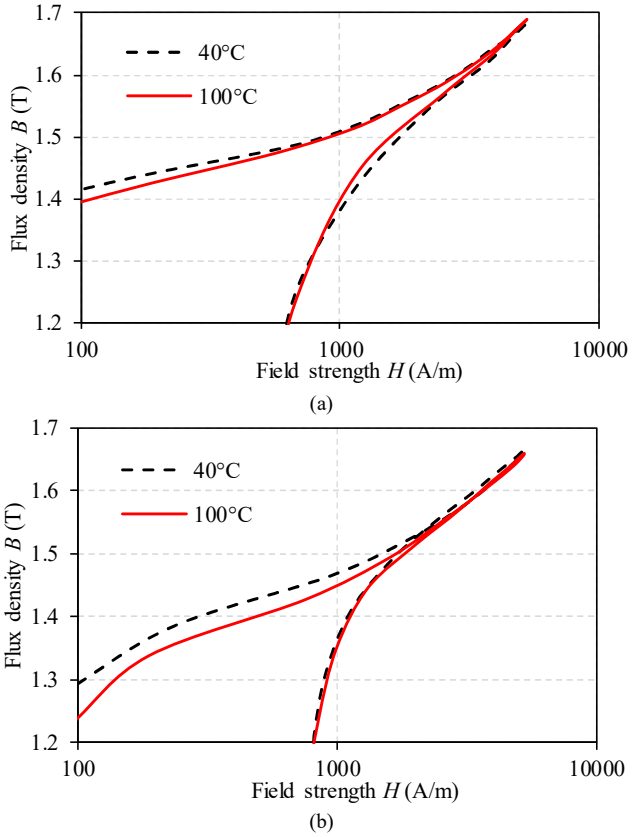

Fig. 4. *B-H* curves at different frequencies and temperatures when flux density is sinusoidal on flux density saturation level. (a) 50Hz. (b) 1000Hz.

III. Iron Loss Models under Constant Temperature

It is important to separate the iron loss contributions according to their origins in iron loss modelling. The principle of the iron loss separation models is finding out the origins of loss contributions firstly, then modelling each loss contribution according to their characters in an engineering way. The iron loss separation makes it easier to understand the iron loss mechanism. Investigations on behaviors of different iron loss contributions also provide more practical ways to model the iron loss. The iron loss of magnetic materials can be concluded as the sum of hysteresis and dynamic losses as [1]:

$$p_{\mathrm{Fe}} = p_{\mathrm{h}} + p_{\mathrm{d}} \tag{4}$$

where p_{h} is the hysteresis loss, p_{d} is the dynamic loss.

The hysteresis loss p_{h} is caused by the discontinues magnetization process in the microscopic level and can be obtained by the area of *B-H* loop under DC hysteresis test times the frequency f. The physical origin of the dynamic loss is the Joule loss caused by the flow of eddy currents around moving domain walls [28]. However, it is reported that there are huge differences between calculated results by classical eddy current loss equations and measured results p_{d} [29]. These differences are caused by the additional power loss produced by the domain wall motion, which is not considered in the classical eddy current loss models. Therefore, a concept of excess loss is introduced to explain this additional loss. The dynamic loss p_{h} then represents the sum of these two parts of losses, i.e. the classical eddy current loss p_{cl} and the excess loss p_{exc}.

The classical eddy current loss represents the Joule loss of eddy current regardless of the domain wall motion. The classical eddy current loss p_{cl} is influenced by the electrical properties of the material. The excess loss p_{exc} represents the loss produced by the motion of domain walls when the materials are exposed to varying magnetic field. The excess loss p_{exc} depends on the microstructure parameters of the material [30]-[32]. The iron loss can be then expressed by the three-term formula including the hysteresis loss, the classical loss and the excess loss as:

$$p_{\mathrm{Fe}} = k_{\mathrm{h}} f B_{\mathrm{m}}^{\alpha} + k_{\mathrm{cl}} f^2 B_{\mathrm{m}}^2 + k_{\mathrm{exc}} f^{1.5} B_{\mathrm{m}}^{1.5} \tag{5}$$

where B_{m} is the amplitude of the flux density. k_{h} and α are the hysteresis loss coefficients. k_{cl} is the classical eddy current loss coefficient. k_{exc} is the excess loss coefficient. The coefficients can be obtained by the curve fitting of the test results at different flux density and frequency.

In [2], the hysteresis loss coefficients k_{h} and α are obtained by fitting the hysteresis loss test result under a DC hysteresis test. The classical eddy current loss is calculated by the properties of the steel laminations. The excess loss coefficient k_{exc} can be obtained by the curve fitting of the test results. The iron loss model can be expressed as:

$$p_{\mathrm{Fe}} = k_{\mathrm{h}} f B_{\mathrm{m}}^{\alpha} + \frac{\sigma d^2}{12}\frac{1}{T}\int_0^T \left(\frac{dB}{dt}\right)^2 dt + \frac{k_{\mathrm{exc}}}{T}\int_0^T \left|\frac{dB}{dt}\right|^{1.5} dt \tag{6}$$

where σ and d are the electrical conductivity and the thickness of the lamination. T is the time period.

It is concluded in [3] that, by the Epstein frame test, the contributions of classical eddy current loss and excess loss cannot be separated. Eight different materials are investigated with a flux density from 0.7T up to 1.7T and frequency from 10Hz up to 150Hz. Zero excess loss coefficient is then identified. A two-term iron loss model is developed. It should be noted that the zero excess loss coefficient in this model does not mean that the actual excess loss is zero. It provides an engineering method to consider the classical eddy current loss and excess losses as a combined global eddy current. This model is also applied widely due to its good applicability [4] [17] [33]. This model can be expressed as:

$$p_{\mathrm{Fe}} = k_{\mathrm{h}} f B_{\mathrm{m}}^2 + k_{\mathrm{e}} f^2 B_{\mathrm{m}}^2 \tag{7}$$

where k_{e} is the global eddy current coefficient.

According to the investigation on the iron loss, the hysteresis loss and eddy current loss coefficients vary with frequency and flux density. The variable hysteresis loss coefficient is reported in [32] [33] and [34]. This can be explained by that the area of the hysteresis loop is influenced by the dynamic losses [5] [37]. The magnetic domains at the microscopic level is a nonlinear and complicated function of both magnetization and frequency [4]. On the other hand, the variation of eddy current coefficient is mainly due to influence of skin effect. The skin effect is frequency and permeability dependent, and the permeability of magnetic material is significantly affected by the flux density [36]. Therefore, an iron loss model with variable coefficients is presented in [4]:

$$p_{\mathrm{Fe}} = k_{\mathrm{h}}(f, B_{\mathrm{m}}) f B_{\mathrm{m}}^2 + k_{\mathrm{e}}(f, B_{\mathrm{m}}) f^2 B_{\mathrm{m}}^2 \tag{8}$$

In order to simplify the modelling of the coefficients, the variation of coefficients with the frequency is considered by using two sets of results representing the low and high frequency regions. In this study, the low frequency covers 50Hz, 200Hz and 400Hz whilst the high frequency covers 600Hz, 800Hz and 1000Hz. This method is also used in [4].

It can be seen from the iron loss models (5)-(8) that the coefficients are very important for the prediction accuracy. The iron loss coefficients are constants in models (5), (6) and (7) while the coefficients are variables in model (8). Table II lists the coefficients for iron loss models (5), (6) and (7). Fig. 5 shows the variable coefficients of iron loss model (8). The values of these coefficients are different from each other due to different obtaining methods. The coefficients in (5) are all obtained by curve fitting of the test results at different alternating flux density and frequency in this study. In (6), the hysteresis loss coefficients k_{h} and α are obtained by fitting the hysteresis loss test result under a DC hysteresis test. The excess loss coefficient k_{exc} is calculated by the curve fitting of the test results under alternating flux density. In (7), the hysteresis loss coefficient k_{h} and the global eddy current loss coefficient k_{e} are calculated by fitting the alternating flux density test results. It should be noted that these coefficients are obtained based on the measured iron loss, generally at a constant temperature. In this section, all the iron loss coefficients are obtained based on the measured results at 40°C.

Fig. 6 shows the relative prediction errors of the iron loss models. Table III shows the numerical results. According to the comparative results, some conclusions can be made as:

a) The accuracies of model (5) and model (6) are similar despite the models are in different forms and the coefficients are obtained by different methods.

b) The two-term model (7) can achieve similar accuracy with the three-term model (5) while the model (7) is easier to implement due to less coefficients.

c) The accuracy of the model (8) is much better than the models (5), (6) and (7) with the help of variable coefficients.

d) The accuracies of (5), (6) and (7) vary significantly at different frequencies and flux densities. This is due to the fact that all these models are based on constant coefficients while the actual iron loss coefficients are flux density and frequency dependent. In other words, iron loss mechanism changes with the frequency. This phenomenon is also reported in [35] and [36]. On the other hand, the prediction accuracy keeps good and stable in the whole test range with the help of variable coefficients.

TABLE II
COEFFICIENTS OF IRON LOSS MODELS (5), (6) AND (7)

Parameters for iron loss model (5)			
k_h	k_{cl}	k_{exc}	α
3.25×10^{-2}	6.67×10^{-5}	5.95×10^{-4}	2
Parameters for iron loss model (6)			
k_h	d (mm)	σ (S/m)	k_{exc}	α
3.6×10^{-2}	3.5×10^{-4}	2.0×10^{6}	5.95×10^{-4}	2
Parameters for iron loss model (7)			
k_h		k_e	
3.76×10^{-2}		8.03×10^{-5}	

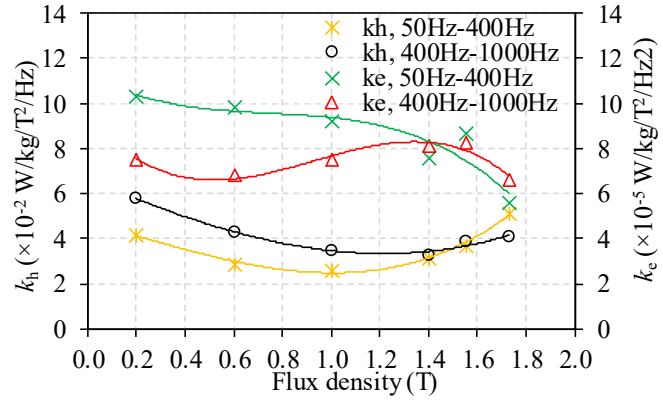

Fig. 5 Coefficients of iron loss model (8).

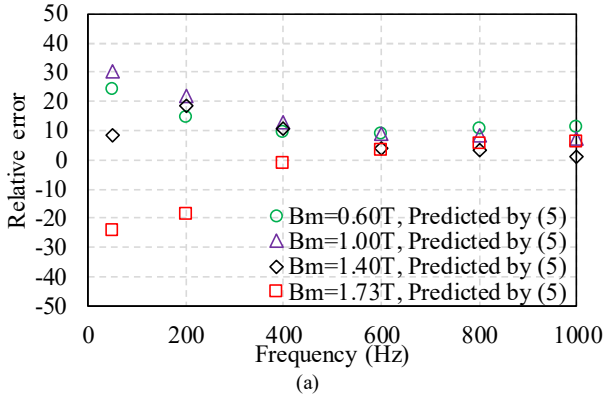

(a)

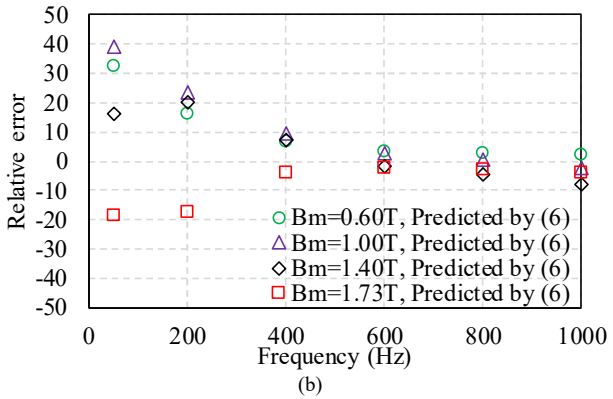

(b)

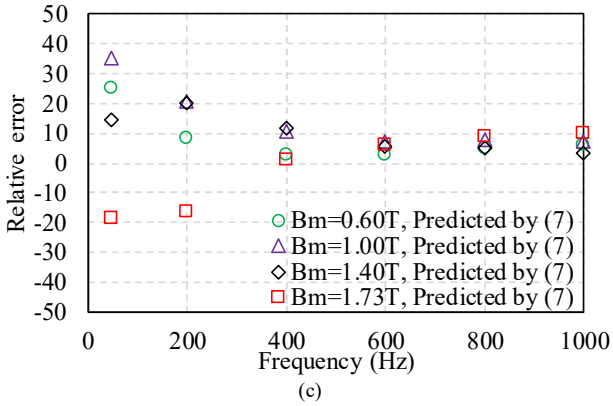

(c)

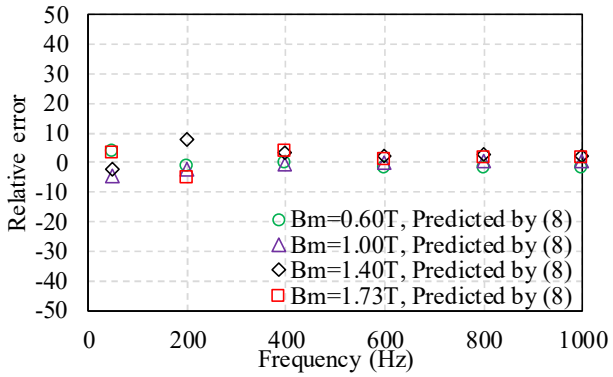

(d)

Fig. 6 Prediction relative errors of iron loss models at 40°C (a) Model (5). (b) Model (6). (c) Model (7). (d) Model (8).

TABLE III
AVERAGE PREDICTION RELATIVE ERROR OF IRON LOSS MODELS AT 40°C

Iron loss model	(5)	(6)	(7)	(8)
Relative error (%)	11.3	10.3	10.7	2.4

IV. IRON LOSS MODELS CONSIDERING TEMPERATURE INFLUENCE

A. Models

According to the comparison in Section III, iron loss model (8) is the most accurate iron loss model with the help of variable coefficients. However, the actual iron loss is temperature dependent. This is due to the hysteresis loss and eddy current loss are dominated by the permeability and resistivity, which are influenced by temperature significantly [8]. Iron loss model (8) cannot consider the influence of temperature on iron loss. One engineering way to solve this problem is to measure the

coefficients of the iron loss model at different temperatures. The iron loss at different temperatures can be then predicted by using these coefficients obtained at different temperatures. However, the coefficients have to be measured at many different temperatures, which is very time consuming. Therefore, different methods to model the temperature dependency of iron loss have been developed in [9] and [10]. In these iron loss models, temperature dependent coefficients are introduced to the existing iron loss models in order to reflect the temperature influence on iron loss. As illustrated in Section III, the iron loss model (8) has the best accuracy when the temperature is constant. Therefore, in this section, different methods for modelling the temperature dependency will be carried out based on iron loss model (8).

As presented in [9], in order to take the temperature influence into account, one method is to consider the temperature dependency of eddy current loss while assuming hysteresis loss is constant. The eddy current loss coefficient is related to the electrical resistivity. The relationship between resistivity and temperature can be expressed as:

$$\rho(T) = \rho_{T_0}[1 + \alpha(T - T_0)] \tag{9}$$

where $\rho(T)$ is the resistivity at temperature T. ρ_{T_0} is the resistivity at the base temperature T_0. α is the temperature coefficient provided by manufacturers. The iron loss model can be expressed as:

$$p_{\mathrm{Fe}} = k_{\mathrm{h}} f B_{\mathrm{m}}^2 + \frac{k_{\mathrm{e}}}{1 + \alpha(T - T_0)} f^2 B_{\mathrm{m}}^2 \tag{10}$$

The temperature dependent of eddy current loss is considered in (10). However, as reported in [8], the hysteresis loss is also influenced by the temperature as the permeability is temperature dependent. Therefore, in [10], an iron loss model is developed to take temperature dependency of both hysteresis and eddy current losses into account. Temperature dependent coefficients are introduced, the iron loss model considering temperature influence can be expressed as:

$$p_{\mathrm{Fe}} = k_{\mathrm{h}}(f, B_{\mathrm{m}}, T) f B_{\mathrm{m}}^2 + k_{\mathrm{e}}(f, B_{\mathrm{m}}, T) f^2 B_{\mathrm{m}}^2 \tag{11}$$

B. Evaluation in Steel Laminations

Fig. 7 shows the prediction relative error of different iron loss models with temperature variation. Table IV shows the average prediction relative errors at 100°C. It can be seen that the relative prediction errors of model (8) increase significantly when the temperature increases. This is due to the coefficients of model (8) are obtained at 40ºC. When the temperature rises, the prediction value is fixed, while the actual iron loss changes. The accuracy of model (10) has shown a slight improvement over that of model (8), with the help of the temperature dependent resistivity. However, the prediction errors of model (10) still vary with the temperature significantly. Iron loss is overestimated or underestimated dramatically when the temperature is high. This is caused by the temperature dependency of hysteresis loss, which is not taken into account in model (10). On the other hand, iron loss model (11) can predict the iron loss with a very low and stable relative prediction error when the temperature changes significantly.

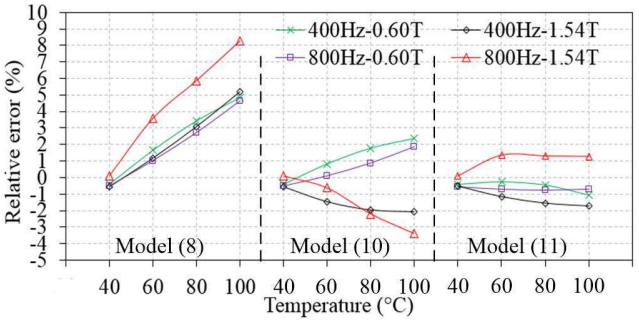

Fig. 7 Prediction relative error of different iron loss models with temperature variation.

TABLE IV
AVERAGE PREDICTION RELATIVE ERROR OF IRON LOSS MODELS AT 100°C

Iron loss model	(8)	(10)	(11)
Relative error (%)	7.5	5.2	2.8

C. Evaluation in an Electrical Machine

In order to evaluate the availability of the iron loss models in electrical machine design, it is necessary to carry out the electrical machine test in this paper. A 12-slot/10-pole interior permanent magnet (IPM) machine is used for the test. The diameters of the machine are listed in Table V. The test system is introduced in this section at first. The iron loss models are then evaluated by comparing the prediction results with the test results. The test system is shown in Fig. 8. The rotor is locked and there is no magnet in the rotor. Therefore, there is no mechanical and magnet eddy current losses in the machine. The three-phase windings are powered by the three-phase AC power source. The measured iron loss of the electrical machine can be obtained by subtracting the copper loss from the total loss. Six thermal couples are equipped at the stator yoke, the coil, the stator tooth, the tooth tip, the rotor magnet slot and the rotor yoke as shown in Fig. 9.

Firstly, the iron losses are measured by applying the pre-tuned input current at room temperature. The iron losses under different currents at room temperature (24°C) can be obtained. Secondly, the electrical machine is heated to the target temperature by its own losses. Fig. 10 shows the temperature variation in different parts of the electrical machine when the phase current is 3.11A in RMS value at 1000Hz. The temperature keeps stable after two hours heating since the heat transfer is almost completed. The hottest part is in the coil (103ºC) and the coolest part is at the stator yoke (99ºC) after heating, the average temperature of different part is 100ºC. The temperature of the electrical machine can be approximately considered as 100ºC. The losses are then measured by applying the pre-tuned input current. Since the measuring process will only take a few seconds, the temperature variation during the measurement can be neglected. The iron losses under different currents at 100ºC can be then obtained by repeating the foregoing process.

The electrical machine is modelled in the FEA software with the measured phase current waveforms. Then, the iron loss is predicted from flux density variations in each FE element using different iron loss models. The temperature dependent losses coefficients for the core are obtained by the ring specimen tests using the same lamination. The measured and predicted iron losses of the electrical machine are compared to evaluate the

model accuracy.

Fig. 11 shows measured and predicted results with different models at 24ºC and 100°C. Table VI shows the relative prediction errors of different iron loss models. The relative prediction errors are obtained by averaging the percentage relative errors at different frequencies. At low frequencies such as 50Hz or100Hz, large prediction errors are found. These are caused by the influences of measuring errors. The iron losses at low frequencies are very small. In this circumstance, even a small measuring error can lead to a huge relative error in percentage. The large relative errors at low frequency increase the average relative errors results. This is the reason that the relative errors listed in Table VI are large. According to the results, the model (8) has the worst accuracy due to the lack of temperature consideration. The accuracy can be improved by applying the model (10). The model (11) has the best accuracy due to the comprehensive consideration on the temperature dependencies of hysteresis and eddy current losses.

TABLE V. PARAMETERS OF ELECTRICAL MACHINE

Stator material	V300-35A	Rotor material	V300-35A
Slot number	12	Tooth body width	7.1mm
Pole number	10	Slot opening	2mm
Stator outer radius	50mm	Stack length	50mm
Stator inner radius	28.5mm	Air gap length	1mm
Rotor outer radius	27.5mm	No. turns per phase	132

TABLE VI. AVERAGE PREDICTION RELATIVE ERROR OF IRON LOSS MODELS AT 100°C IN THE 12/10 IPM

Iron loss model	(8)	(10)	(11)
Relative error (%)	51.7	42.1	29.6

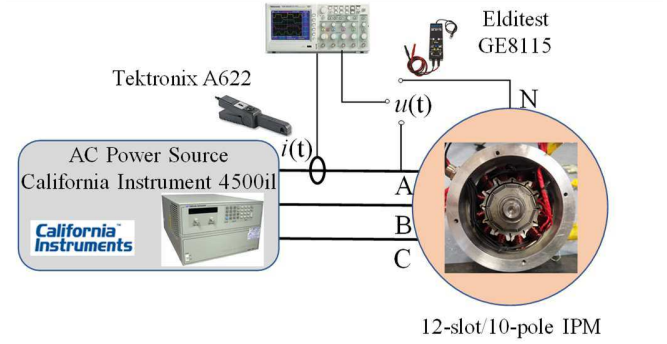

Fig. 8. Locked rotor test without magnets.

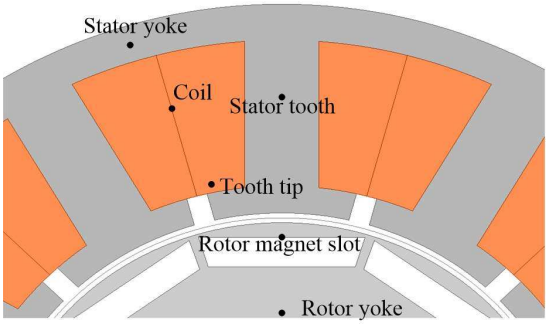

Fig. 9. Thermal couple locations in the electrical machine.

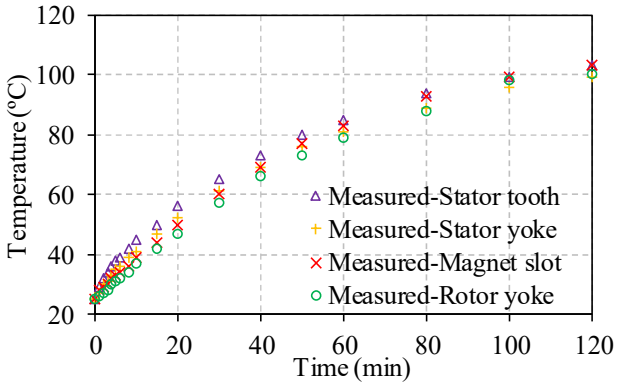

Fig. 10. Temperature variations of different parts of electrical machine when the phase current is 3.11A in RMS value at 1000Hz.

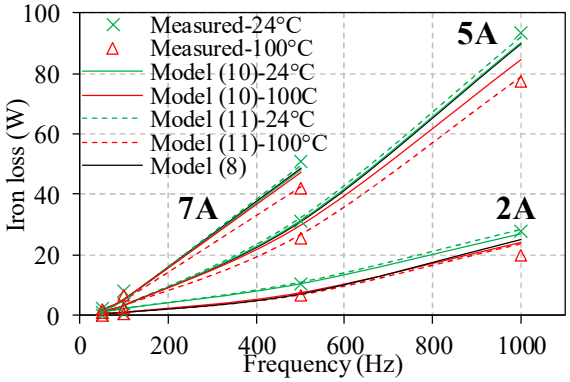

Fig. 11. Measured and predicted results of electrical machine when the temperature is 24ºC and 100ºC.

D. Further Thermal Evaluation of Models for Considering Temperature Influence

In order to evaluate the risk of insulation failure of the winding and demagnetization of the magnets, it is essential to predict the temperature accurately. Iron loss is one of the major sources of temperature rise in electrical machines. Therefore, it is necessary to apply the iron loss models in the electrical machines and evaluate them in terms of the thermal analysis. In this section, thermal analyses are carried out. The 12-slot/10-pole IPM machine introduced in Section IV-C is used for the test. The Motor-CAD software [25] is used for the thermal modelling and analysis of the machine. Fig. 12 shows the thermal model of the 12-slot/10-pole IPM machine.

Fig. 13 shows the thermal analysis methods by different iron loss models. The magnets are removed, and the motor is locked to eliminate the magnet loss and mechanical loss. Therefore, only iron loss and copper loss are included in the input power to the thermal model. Fig. 13(a) shows the thermal analysis method by utilizing the iron loss model (8), where only the temperature dependency of copper loss is considered. The calculated copper loss varies with the temperature change and feedbacks to the input power during the analysis. The iron loss keeps constant during the analysis. On the other hand, the thermal analysis methods by models (10) and (11) are shown in Fig. 13(b). Both the calculated iron loss and copper loss vary with the temperature change and are feedback to the input power during the analysis.

The predicted iron loss results by different analysis methods are shown in Fig. 14. When the temperature rises, the predicted

iron losses by models (10) and (11) decrease while the predicted iron loss by model (8) keeps constant.

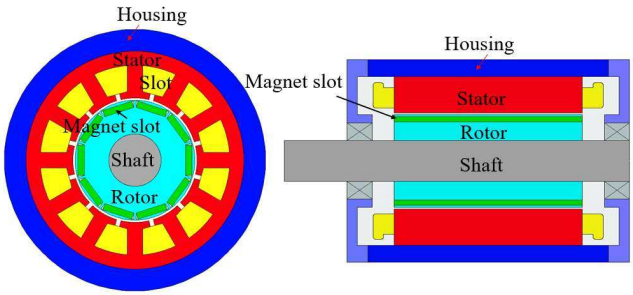

Fig. 12. Thermal model of 12-slot/10-pole IPM machine.

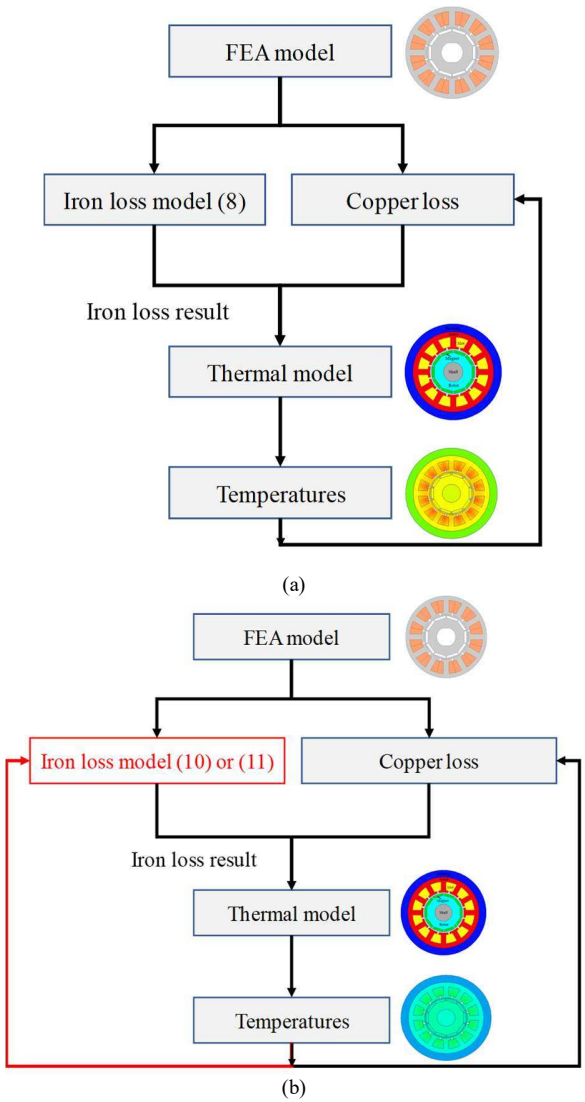

Fig. 13. Thermal analysis methods. (a) Analysis method for model (8). (b) Analysis method for model (10) or (11).

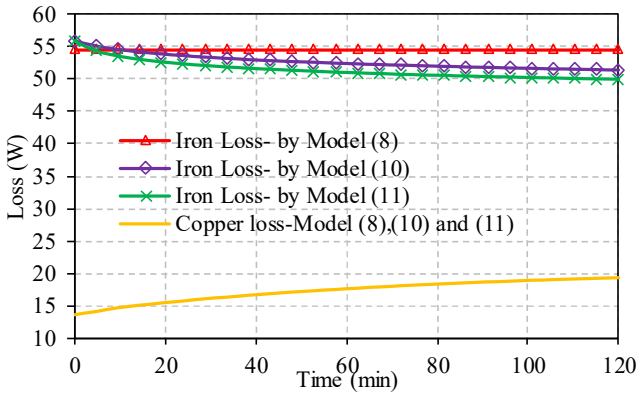

Fig.14. Predicted losses by different thermal analysis methods. Phase current=3.11A RMS, f=1000Hz.

Fig. 15 shows the comparisons of the measured and predicted results by the different analysis methods. The prediction error results at t=120 min are also listed in Table VII. It can be observed that the model (8) has the worst accuracy since the lack of temperature consideration. Both model (10) and model (11) can consider the temperature influence on the iron loss and they obtain better accuracy compared to model (8). The analysis method with model (11) has the best temperature prediction accuracy due to the fact that the model (11) fully considers the flux density, frequency and temperature dependencies of hysteresis and eddy current losses.

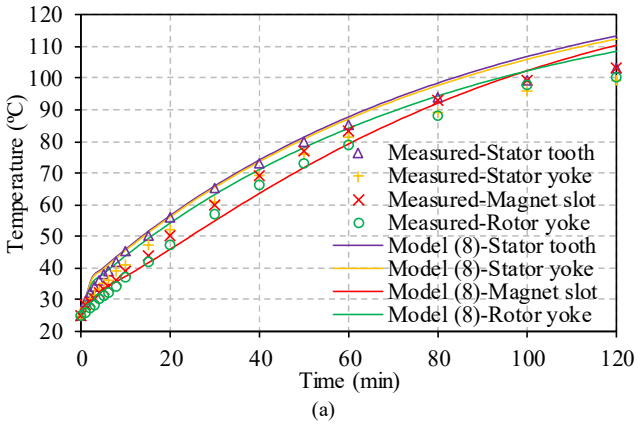

(a)

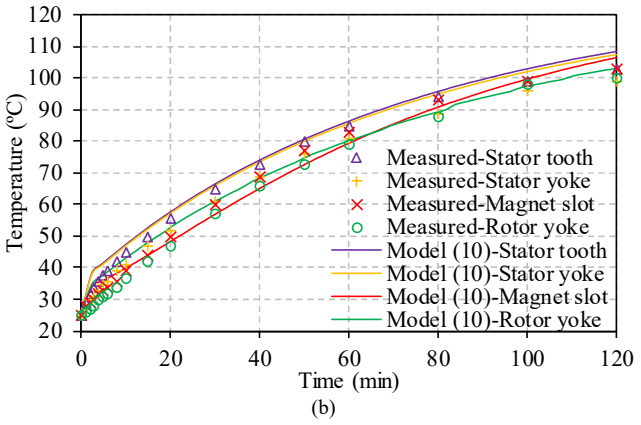

(b)

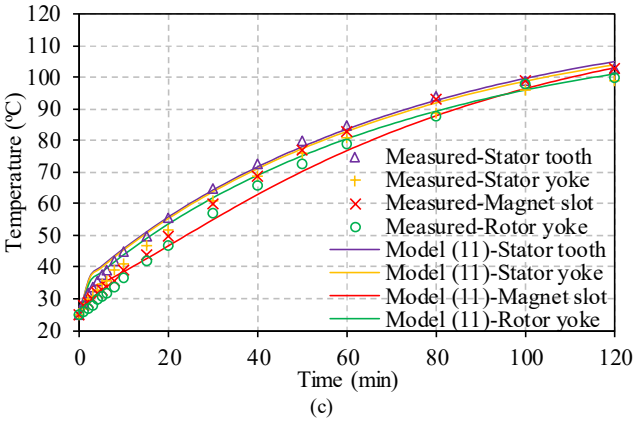

(c)

Fig. 15. Comparison of predicted and measured temperatures by using (a) Existing thermal analysis method with iron loss model (8), and (b) Thermal-loss coupling method with iron loss model (10). (c) Thermal-loss coupling method with iron loss model (11).

TABLE VII. TEMPERATURE PREDICTION ERRORS

Positions	Model (8) (%)	Model (10) (%)	Model (11) (%)
Stator tooth	10.0	5.2	2.0
Stator yoke	13.4	7.9	5.2
Magnet slot	7.2	3.6	0.1
Rotor yoke	8.6	4.5	1.1
Average	**9.8**	**5.3**	**2.1**

V. INFLUENCE OF ROTATIONAL FIELD ON THE IRON LOSS

In electrical machines, the flux density in stator or rotor cores can be rotational. It is widely reported that the rotational flux density causes additional iron loss [17][18][26][27].

In [17], the rotational flux density is decomposed into the *x*-axis and the *y*-axis as shown in Fig. 16. The total iron loss can be then obtained by the sum of iron losses at these two directions as:

$$p_{\mathrm{Fe,Total}} = p_{\mathrm{Fe,x}} + p_{\mathrm{Fe,y}} \tag{12}$$

where $p_{\mathrm{Fe,Total}}$ is the total iron loss under rotational flux density. $p_{\mathrm{Fe,x}}$ and $p_{\mathrm{Fe,x}}$ are the iron loss calculated by the alternating flux density on *x*-axis and *y*-axis, respectively.

In [18], the rotational flux density is decomposed into the major-axis and minor-axis as shown in Fig. 16 instead of the *x*-axis and the *y*-axis. The iron loss can be then expressed as:

$$p_{\mathrm{Fe,Total}} = p_{\mathrm{Fe,major}} + p_{\mathrm{Fe,minor}} \tag{13}$$

where $p_{\mathrm{Fe,major}}$ and $p_{\mathrm{Fe,minor}}$ are the iron losses calculated by the alternating flux density along the major-axis and the minor-axis, respectively.

In order to evaluate different methods for considering rotational flux density, an electrical machine test is carried out. The electrical machine test procedure is introduced in Section IV-C. The FEA model of the machine is also built. The flux density in each element of the FEA model is decomposed to different directions after it is solved, i.e. *x*-*y*-axes for the model (12) or major-minor axes for the model (13). The iron loss of each axis is calculated by model (11). The total rotational iron losses can be then calculated by summing the losses at *x*-*y* or major-minor axes, respectively. The different models are then evaluated by the comparison between the predicted and measured results.

Fig. 17 shows the measured and predicted iron losses at different temperatures by different methods. The model (13) considering the rotational flux density on major-minor axis has a better accuracy compare to model (12).

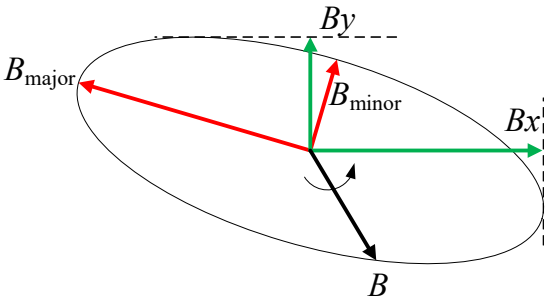

Fig. 16. Rotational flux density loci.

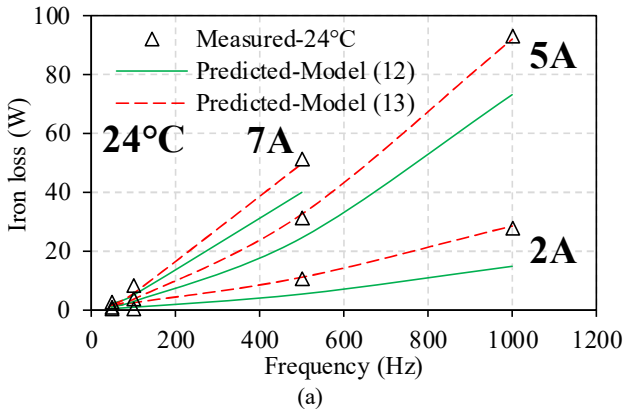

(a)

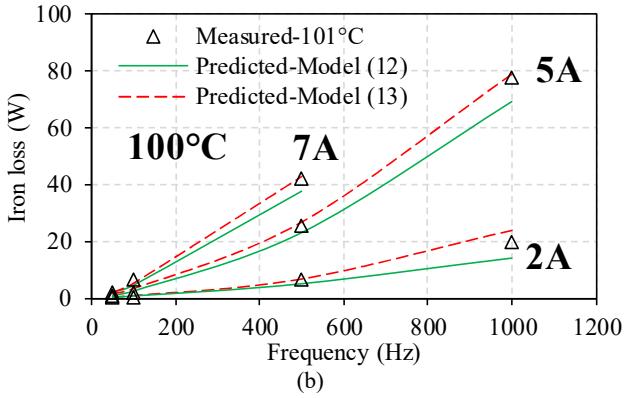

(b)

Fig. 17. Measured and predicted results using different methods, with iron loss of each axis is calculated by model (11). (a) 24°C. (b) 100°C.

VI. IRON LOSS MODEL FOR NON-SINUSOIDAL FLUX DENSITY

The iron loss models discussed in Sections III, IV and V are based on the assumption that the flux density waveform is sinusoidal. However, in actual electrical machines, the flux density can be different from sinusoidal. On one hand, the DC bias flux density exists in many types of electrical machines such as permanent-magnet synchronous machine (PMSM), brushless DC machine (BLDC) and switched reluctance machine (SRM), etc. More importantly, DC bias flux density can significantly influence the iron loss [11]-[13]. On the other hand, electrical machines are usually powered by PWM inverters. The current waveform of electrical machines can be significantly distorted from sinusoidal. This can result in

significant fluctuation of flux density in electrical machines and then additional iron losses [14]-[16].

In this section, different iron loss models for consideration of the flux density with DC bias and for electrical machine fed by PWM inverters are evaluated against the measured iron loss in the electrical machine.

A. Iron Loss Models for Flux Density with DC Bias

The iron loss model developed in [11] is one of the most widely used iron loss models considering the influence of DC bias flux density as:

$$p_{\mathrm{Fe}} = \varepsilon(B_{\mathrm{bias}})k_{\mathrm{h}} f B_{\mathrm{m}}^2 + k_{\mathrm{e}} f^2 B_{\mathrm{m}}^2 \tag{14}$$

$$\varepsilon(B_{\mathrm{bias}}) = 1 + k_{\mathrm{DC}} B_{\mathrm{bias}}^{\alpha} \tag{15}$$

where p_{Fe} is the iron loss. $\varepsilon(B_{\mathrm{bias}})$ is the ratio between hysteresis losses with and without DC bias flux density. k_{h} and k_{e} are the hysteresis and eddy current losses coefficients, respectively. f is the frequency of AC flux density. B_{m} is the amplitude of AC flux density. k_{DC} and α are the DC bias coefficients and can be obtained by steel lamination tests.

According to the investigation in [13], the coefficient $\varepsilon(B_{\mathrm{bias}})$ is not only the DC bias flux density but also the temperature dependent. Furthermore, hysteresis and eddy current loss coefficients k_{h} and k_{e} are also flux density, frequency and temperature dependent as illustrated in Section IV. Therefore, an iron loss model considering the temperature dependence of flux density, frequency and DC bias flux density is developed in [13] as:

$$p_{\mathrm{Fe},T} = \varepsilon(B_{\mathrm{bias}}, T)k_{\mathrm{h}}(f, B_{\mathrm{m}}, T) f B_{\mathrm{m}}^2 + k_{\mathrm{e}}(f, B_{\mathrm{m}}, T) f^2 B_{\mathrm{m}}^2 \tag{16}$$

$$\varepsilon(B_{\mathrm{bias}}, T) = 1 + k_{\mathrm{DC}}(T) B_{\mathrm{bias}}^{\alpha(T)} \tag{17}$$

Fig. 18 shows measured DC bias coefficients k_{DC} and α at different temperatures. Both k_{DC} and α vary almost linearly with the temperature for the investigated temperature range. Thus, with k_{DC} and α obtained based on measured iron losses at two different temperatures, they can be used to predict the iron loss at the other temperatures.

In order to evaluate the iron loss models for flux density with DC bias, tests on the electrical machine are carried out. The 12-slot/10-pole IPM machine used in Section V is also used in this section. However, instead of removing magnets from the rotor, permanent magnets are installed in the rotor to generate DC bias flux density. Ferrite magnets are used due to its negligible eddy current loss. Fig. 19 shows the measured and predicted iron losses in the electrical machine. It can be seen that the iron loss at 19°C and 101°C varies significantly while the predicted results of iron loss model (14) keep constant. On the other hand, the iron loss model (16) can track this variation with the help of temperature dependent coefficients.

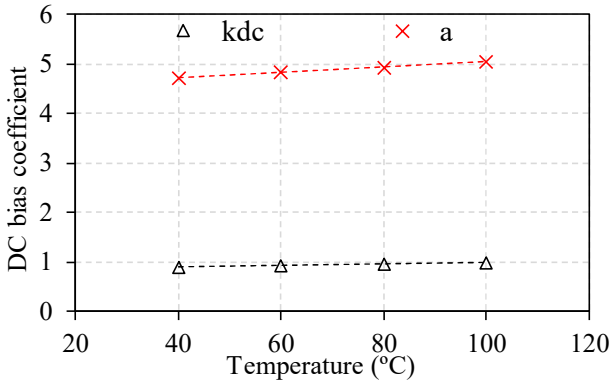

Fig.18. DC bias coefficients variation with temperature.

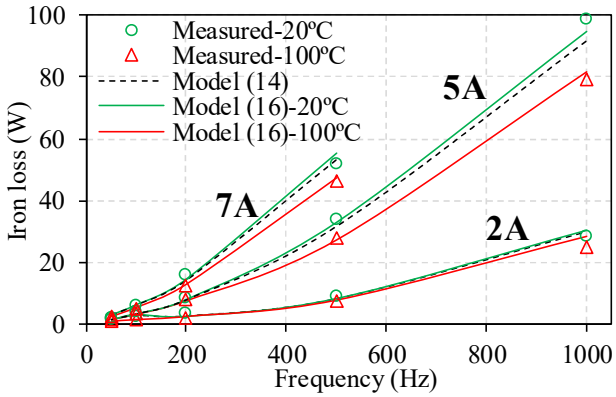

Fig.19. Measured and predicted iron losses by different models.

B. Iron Loss Model for Electrical Machine Fed by PWM Inverters

When the electrical machine is fed by PWM inverter, the phase current waveform can be significantly distorted from sinusoidal. This distorted current will cause flux density fluctuations in the electrical machine. The hysteresis minor loops occur as shown in Fig. 20, the iron loss is then influenced. In order to explain this influence more clearly, *B-H* loops at different switching frequencies are tested in the ring specimen. Fig. 21 shows measured *B-H* loops at different switching frequencies and temperatures at fundamental frequency 1Hz and flux density amplitude 1.20T. It can be seen that *B-H* loops can be dramatically distorted when the switching frequency is low. The shape of *B-H* loops is also influenced by temperature. The iron loss is then affected. On the other hand, the harmonics of the distorted flux density also cause additional eddy current iron loss. Therefore, in [16], an iron loss model for electrical machine fed by PWM inverter is developed:

$$p_{\mathrm{Fe}} = k_{\mathrm{minor}} k_{\mathrm{h}}(f, B_{\mathrm{m}}, T) f B_{\mathrm{m}}^2 + \sum k_{\mathrm{e}}(f, B_{\mathrm{m}}, T) f^2 B_{\mathrm{m}}^2 \tag{18}$$

$$k_{\mathrm{minor}} = 1 + k \frac{1}{B_{\mathrm{m}}} \sum_{i=1}^{N} \Delta B_i \tag{19}$$

where k_{minor} is the coefficient considering the influence of hysteresis minor loops. k is the coefficient depending on lamination properties. ΔB_i is the amplitude of the flux density fluctuations shown in Fig. 20.

In order to evaluate the iron loss models for electrical machines fed by PWM inverter. Two sets of tests are carried out in this section. One is conducted when the 12-slot/10-pole IPM machine is powered by an inverter controlled by a

dSPACE controller at different switching frequencies. The other one is carried out when the machine is powered with sinusoidal current by the three-phase current source California Instrument 4500il. For each iron loss test, the RMS value of the phase current is kept the same.

Fig. 22 shows the measured and predicted results at different switching frequencies when the fundamental frequency is 50Hz and 100Hz, respectively. It can be seen that when the electrical machine is powered by sinusoidal current, both of the models (11) and (18) can accurately predict the iron loss. When the switching frequency decreases, the iron loss increases significantly. The iron loss model (11) cannot reflect this variation due to the lack of the consideration of minor loops and eddy current harmonics. On the other hand, the iron loss model (18) keeps good accuracy even when the switching frequency is very low.

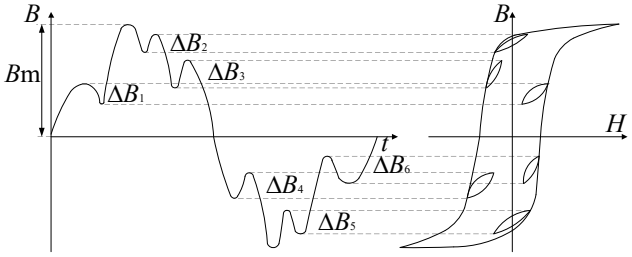

Fig.20. Flux density distortion in electrical machine when supplied by PWM inverter.

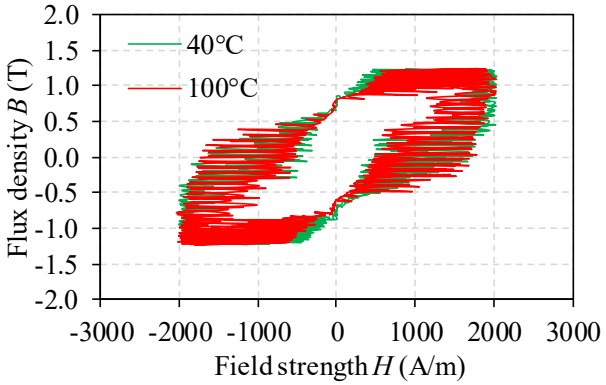

(a)

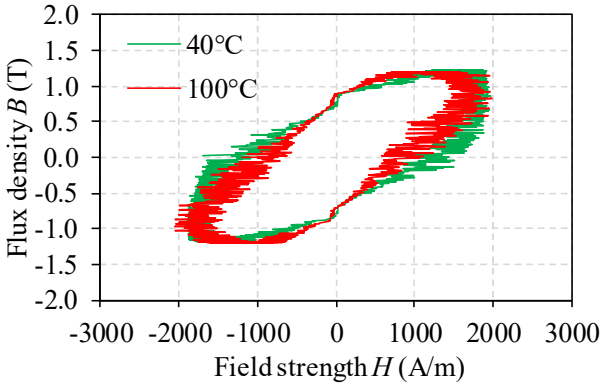

(b)

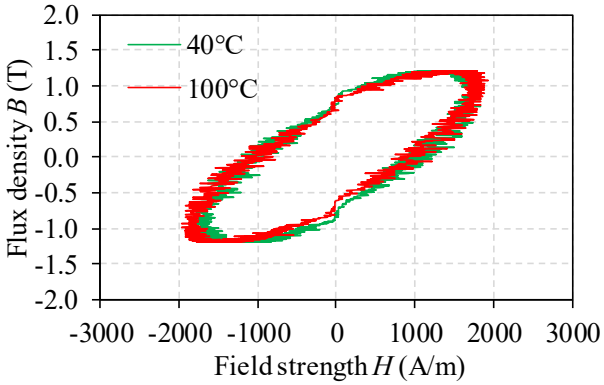

(c)

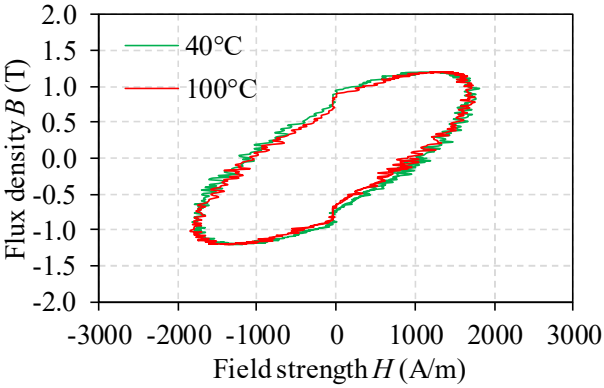

(d)

Fig.21. *B-H* loops at different switching frequencies f_s and temperatures when the fundamental frequency f=1Hz, B_m=1.20T. (a) f_s=500Hz. (b) f_s=2kHz. (c) f_s=5kHz. (d) f_s=10kHz.

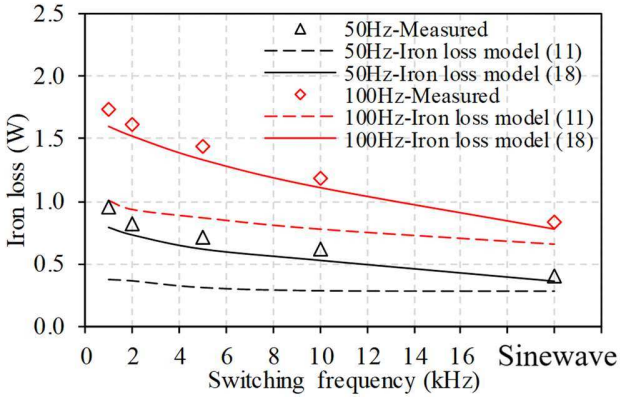

Fig.22. Comparison of measured and predicted results.

VII. Conclusions

In this paper, more than ten iron loss models are comprehensively evaluated against the measured iron losses considering alternating and rotating fields, temperature influence, flux density with DC bias and flux density fluctuation caused by PWM inverter. Some conclusions can be highlighted as below:

1) The iron loss model (8) developed in [4] has the best accuracy when the flux density is alternating sinusoidally at constant temperature with the help of variable coefficients.

2) The iron loss model (11) has the best accuracy for considering the temperature variation

3) It is more accurate to calculate the iron loss under rotational flux density by decomposing the flux density into major-minor axis than into *x*-*y* axis.

4) The iron loss model (16) can accurately predict iron loss under flux density with DC bias at different temperatures while taking the temperature influence into account.

5) The iron loss model (18) can effectively consider the additional iron loss caused by PWM inverter in the electrical machine.

REFERENCES

[1] G. Bertotti, "General properties of power losses in soft ferromagnetic materials," *IEEE Trans. Magn*., vol. 24, no. 1, pp. 621-630, Jan. 1988.

[2] K. Atallah, Z. Q. Zhu, and D. Howe, "An improved method for predicting iron losses in brushless permanent magnet DC drives," *IEEE Trans. Magn*., vol. 28, no. 5, pp. 2997-2999, Sep. 1992.

[3] A. Boglietti, A. Cavagnino, M. Lazzari, and M. Pastorelli, "Predicting iron losses in soft magnetic materials with arbitrary voltage supply: an engineering approach", *IEEE Trans. Magn*., vol. 39, no. 2, pp. 981-989, Mar. 2003.

[4] D. M. Ionel, M. Popescu, M. I. McGilp, T. J. E. Miller, S. J. Dellinger, and R. J. Heideman, "Computation of core losses in electrical machines using improved models for laminated steel," *IEEE Trans. Ind. Appl.*, vol. 43, no. 6, pp. 1554-1564, Nov./Dec. 2007.

[5] F. Fiorillo, A. Novikov, "An improved approach to power losses in magnetic laminations under nonsinusoidal induction wave-form," *IEEE Trans. Magn*., vol. 26, no. 5, pp. 2904-2910, Sep. 1990.

[6] O. Barriere, C. Appino, F. Fiorillo, C. Ragusa, M. Lecrivain, L. Rocchino, H. Ben Ahmed, M. Gabsi, F. Mazaleyrat, and M. LoBue, "Characterization and prediction of magnetic losses in soft magnetic composites under distorted induction waveform," *IEEE Trans. Magn*., vol. 49, no. 4, pp. 1318-1326, Apr. 2013.

[7] M. Cossale, A. Krings, J. Soulard, A. Boglietti and A. Cavagnino, "Practical investigations on cobalt-iron laminations for electrical machines," *IEEE Trans. Ind. Appl*., vol. 51, no. 4, pp. 2933-2939, Jul./Aug. 2015.

[8] N. Takahashi, M. Morishita, D. Miyagi, and M. Nakano, "Examination of magnetic properties of magnetic materials at high temperature using a ring specimen," *IEEE Trans. Magn*., vol. 46, no. 2, pp. 548-551, Feb. 2010.

[9] J. Chen, D. Wang, S. Cheng, Y. Wang. Y. Zhu, Q. Liu, "Modeling of temperature effects on magnetic property of nonoriented silicon steel lamination," *IEEE Trans. Magn*., vol.51, no.11, pp. 1-4, Nov. 2015.

[10] S. Xue, J. Feng, S. Guo, J. Peng, W. Q. Chu, and Z.Q. Zhu, "A new iron loss model considering temperature influences of hysteresis and eddy current losses separately in electrical machines," *IEEE Trans. Magn*., vol. 54, no. 1, pp. 1-10, Jan. 2018.

[11] C. Simao, N. Sadowski, N. J. Batistela, and J. P. A. Bastos, "Evaluation of hysteresis losses in iron sheets under DC-biased inductions," *IEEE Trans. Magn.*, vol. 45, no. 3, pp. 1158-1161, Mar. 2009.

[12] S. Zhu, M. Cheng, J.N. Dong, and J. Du, "Core loss analysis and calculation of stator permanent-magnet machine considering dc-biased magnetic induction," *IEEE Trans. Ind. Electron.*, vol. 61, no. 10, pp. 5203-5212, Jan. 2014.

[13] S. Xue, J. Feng, S. Guo, Z. Chen, J. Peng, W. Q. Chu, L. R. Huang, Z. Q. Zhu, "Iron loss model under DC bias flux density considering temperature influence," *IEEE Trans. Magn*., vol. 53, no. 11, pp. 1-4, Nov. 2017.

[14] J. Lavers, P. Biringer, and H. Hollitscher, "A simple method of estimating the minor loop hysteresis loss in thin laminations," *IEEE Trans. Magn.*, vol. 14, no.5, pp. 386-388, Sep. 1978.

[15] S. Calverley, G. Jewell, and R. Saunders, "Prediction and measurement of core losses in a high-speed switched-reluctance machine," *IEEE Trans. Magn*., vol. 41, no. 11, pp. 4288-4298, Nov. 2005.

[16] S. Xue, J. Feng, S. Guo, Z. Chen, J. Peng, W. Q. Chu, P. L. Xu, Z. Q. Zhu, "Iron loss model for electrical machine fed by low switching frequency inverter," *IEEE Trans. Magn*., vol. 53, no. 11, pp. 1-4, Nov. 2017

[17] M. Enokizono, T. Suzuki, J. Sievert, and J. Xu, "Rotational power loss of silicon steel sheet," *IEEE Trans. Magn.*, vol. 26, no. 5, pp. 2562-2564, Sep. 1990.

[18] R. Findlay, N. Stranges, and D. K. MacKay, "Losses due to rotational flux in three phase induction motors," *IEEE Trans. Energy Conversion*, vol. 9, no.3, pp. 543–549, Sep. 1994.

[19] Z. Q. Zhu, S. Xue, J. Feng, S. Guo, Z. Chen, J. Peng, and W. Q. Chu, "Evaluation of iron loss models in electrical machines," in *International Conference on Electrical Machines and Systems (ICEMS)* Sydney, Australia, Aug. 2017, pp. 1-4.

[20] A. Moses and S. Hamadeh, "Comparison of the Epstein-square and a single-strip tester for measuring the power loss of nonoriented electrical steels," *IEEE Trans. Magn.*, vol. 19, no. 6, pp. 2705-2710, Nov. 1983.

[21] A. Espíndola, F. Tristão, J. P. Schlegel, N. J. Batistela, N. Sadowski, P. Kuo-Peng, M. Rigoni, "Comparison of iron losses evaluations by different testing procedures," in *Elect. Mach. 2010 XIX Int. Conf.*, Rome, Italy, Sept. 2010, pp. 1-4.

[22] A. Krings and J. Soulard, "Experimental characterization of magnetic materials for electrical machine applications," in *IEEE Elect. Mach. Design, Control and Diagnosis Workshop*, Torino, Italy, Mar. 2015, pp. 85-89.

[23] J. Muhlethaler, J. Biela, J. W. Kolar, and A. Ecklebe, "Core losses under the DC bias condition based on Steimetz parameters," *IEEE Trans. Power Electron*., vol. 27, no. 2, pp. 953-963, Feb. 2012.

[24] L. K. Rodrigues and G. W. Jewell, "Model specific characterization of soft magnetic materials for core loss prediction in electrical machines," *IEEE Trans. Magn*., vol. 50, no. 11, pp. 1-4, Nov. 2014.

[25] Motor-CAD. Available online: https://www.motor-design.com.

[26] J. G. Zhu and V. S. Ramsden, "Improved formulations for rotational core losses in rotating electrical machines," *IEEE Trans. Magn*., vol. 34, no. 4, pp. 2234-2242, Jul. 1998.

[27] Y. K. Huang, J. N. Dong, J. G. Zhu, and Y. G. Guo, "Core loss modeling for permanent-magnet motor based on flux variation locus and finite-element method," *IEEE Trans. Magn.*, vol. 48, no. 2, pp. 1023-1026, Feb. 2012.

[28] J. Shilling and G. Houze, "Magnetic properties and domain structure in grain-oriented 3% Si-Fe," *IEEE Trans. Magn*., vol. 10, no. 2, pp: 195-223, Jun. 1974.

[29] C. D. Graham Jr., "Physical origin of losses in conducting ferromagnetic materials," *J. Appl. Phys*., vol. 53, no. 11, pp: 8276-8280, Aug. 1998.

[30] I. Mayergoy and C. Serpico, "Nonlinear diffusion of electromagnetic fields and excess eddy current losses," *J. Appl. Phys*., vol. 85, no. 8, pp: 4910-4912, Apr. 1999.

[31] C. Serpico, C. Visone, I. Mayergoy, V. Basso and G. Miano "Eddy current losses in ferromagnetic laminations," *J. Appl. Phys*., vo. 87, no. 9, pp: 6923-6925, Apr. 2000.

[32] Y. Zhang, P. Pillay, M. Ibrahim and M. C. Cheng, "Magnetic characteristics and core losses in machine laminations: high-frequency loss prediction from low-frequency measurements," *IEEE Trans. Ind. Appl*., vo. 48, no. 2, pp: 623-629, Dec. 2011.

[33] H. Domeki, Y. Ishihara, C. Kaido, Y. Kawase, S. Kitamura, T. Shimomura, N. Takahashi, T. Yamada and K. Yamazaki, "Investigation of benchmark model for estimating iron loss in rotating machine," *IEEE Trans. Magn*., vo. 40, no. 2, pp: 794-797, Mar. 2004.

[34] J. R. Hendershot and T. J. E. Miller, *Design of Brushless Permanent Magnet Motors*. Mentor, OH: Magna Physics, 1994.

[35] E. Barbisio, F. Fiorillo and C. Ragusa, "predicting loss in magnetic steels under arbitrary induction waveform and with minor hysteresis loops," *IEEE Trans. Magn*., vol. 40, no. 4, pp. 1810-1819, Jul 2004.

[36] J. Barranger, "Hysteresis and eddy-current losses of a transformer lamination viewed as an application of the poynting theorem," *NASA tn d-3114, NASA technical note*, Lewis Research Center, Cleveland, Ohio, Nov. 1965.

[37] G. Bertotti, A. A. Boglietti, M. Chiampi, D. Chiarabaglio, and F. Fiorillo, "An improved estimation of iron loss in rotating electrical machines," *IEEE Trans. Magn*., vol. 27, no. 6, pp. 5007-5009, Nov. 1991.

Z.Q. Zhu (M'90–SM'00–F'09) received the B.Eng. and M.Sc. degrees in electrical engineering from Zhejiang University, Hangzhou, China, in 1982 and 1984, respectively, and the Ph.D. degree in electrical and electronic engineering from The University of Sheffield, Sheffield, U.K., in 1991.

Since 1988, he has been with the University of Sheffield, where since 2000, he has been a Professor with the Department of Electronic and Electrical Engineering. He is currently the Royal Academy of Engineering/Siemens Research Chair, and the Head of the Electrical Machines and Drives Research Group, the Academic Director of Sheffield Siemens Wind Power Research Centre, the Director of CRRC Electric Drives Technology Research Centre, and the Director of Midea Electric Machines and Controls Research Centre. His current major research interests include the design and control of permanent magnet brushless machines and drives for applications ranging from automotive to renewable energy. He has received ~30 Best Paper Awards, including 6 IEEE Transactions and IET Proceedings Prize Paper Awards. He is a Fellow of Royal Academy of Engineering and a Fellow of Institute of Engineering and Technology, U.K.

Shaoshen Xue received the B. Eng. and M. Sc. degrees in electrical engineering from Southeast University, Nanjing, China in 2009 and Beijing Jiaotong University, Beijing, China in 2011, respectively, and the Ph.D. degree in the electronic and electrical engineering from The University of Sheffield, UK, in 2017.

From 2011 to 2013, he was with Institute of Electrical Engineering, Chinese Academy of Science. From 2013 to 2014, he was with Beijing Benz Automotive Ltd. He is currently a postdoctoral research associate at Sheffield-Siemens Wind Power Research Centre. His major research interests are electrical machine design and control for applications including automotive and renewable energy.

Wenqiang Chu received the B. Eng. and M. Sc. degrees in electrical engineering from Zhejiang University, Hangzhou, China in 2004 and Huazhong University of Science and Technology, Wuhan, China in 2007, respectively, and the Ph.D. degree in the electronic and electrical engineering from The University of Sheffield, UK, in 2013.

From 2007 to 2009, he was with Delta Electronics (Shanghai) Co. Ltd. From 2012 to 2014, he was a postdoctoral research associate with The University of Sheffield. From 2014 to 2017, he was a principal design engineer with CRRC Electric Drive Technology Research Centre, The University of Sheffield, UK. Currently, he is deputy CTO of INOVANCE Technology Co., Ltd. His major research interests include electric drive systems and applications.

Jianghua Feng (S'06) received his B.S. and M.S. degrees in Electrical Machinery Control from Zhejiang University, China in 1986 and 1989, respectively, and Ph. D. degree in Control Theory and Control Engineering from Central South University, China in 2008. Since 1989, he has been with CRRC Zhuzhou Institute Co. Ltd., Zhuzhou, China, where he is presently the Vice President and Chief Technology Officer. He has published a number of journal and conference proceedings papers. His research interests are modeling, control, and communication of electrical systems, rail networks and high-speed trains. He is also a Guest Professor in Southwest Jiaotong University, Tongji University and Central South University.

Shuying Guo is a professorial senior engineer. She graduated from Central South University in December 1981, and serves as the chief technical expert in CRRC Zhuzhou Institute Co., Ltd. in the field of R&D of the electric machine systems for railway locomotive and electrical vehicle applications.

Zhichu Chen received the B.Eng. degree in electrical engineering and automation from Southwest Jiaotong University, Chengdu, China, in 2005, and the M.Sc. degree in electrical engineering from Zhejiang University, Hangzhou, China, in 2016. Since 2005, he has been with CRRC Zhuzhou Institute Co., Ltd., Zhuzhou, China. His major research interests include design and application of electric machine and drive system.

Jun Peng received the B.Eng. degree in mechanical design from Huazhong Agricultural University, Wuhan, China, in 2007, and the M.Sc. degree in electrical engineering from Huazhong University of Science and Technology, Wuhan, China, in 2016. Since 2007, he has been with CRRC Zhuzhou Institute Co., Ltd., Changsha, China. His major research interests include design and application of permanent magnet machines for electrical vehicle application.